



Pulse dynamics in low-Reynolds-number interfacial hydrodynamics: Experiments and theory

D. Tseluiko^a, S. Saprykin^a, C. Duprat^b, F. Giorgiutti-Dauphiné^b, S. Kalliadasis^{a,*}

^a Department of Chemical Engineering, Imperial College London, London SW7 2AZ, United Kingdom

^b Université Paris-Sud, UPMC, Lab FAST, Bat 502, Campus Universitaire, Orsay 91405, France

ARTICLE INFO

Article history:

Received 23 July 2009

Received in revised form

7 July 2010

Accepted 24 July 2010

Available online 30 July 2010

Communicated by K. Promislow

Keywords:

Kuramoto–Sivashinsky equation

Solitary pulse interaction

Bound states

ABSTRACT

We analyze interaction of nonlinear pulses in active–dispersive–dissipative nonlinear media. A particular example of such media is a viscous thin film coating a vertical fibre. Experiments for this system reveal that the interface evolves into a train of droplike solitary pulses in which numerous inelastic coalescence events take place. In such events, larger pulses catch up with smaller ones and annihilate them. However, for certain flow conditions and after a certain distance from the inlet, no more coalescence is observed and the flow is described by quasi-equilibrium solitary pulses interacting continuously with each other through attractions and repulsions, and, eventually they form bound states of groups of pulses in which the pulses travel with the same velocities as a whole. This experimental study represents the first evidence of formation of bound states in low-Reynolds-number interfacial hydrodynamics. To gain theoretical insight into the interaction of the pulses and formation of bound states, we derive a weakly nonlinear model for the flow, the generalized Kuramoto–Sivashinsky (gKS) equation, that retains the fundamental mechanisms of the wave evolution, namely, dominant nonlinearity, instability, stability and dispersion. Much like in the experiments, the spatio-temporal evolution of the gKS equation is dominated by quasi-stationary solitary pulses which continuously interact with each other through coalescence events or attractions/repulsions. To understand the latter case, we utilize a weak-interaction theory for the solitary pulses of the gKS equation. The theory is based on representing the solution of the equation as a superposition of the pulses and an overlap function and leads to a coupled system of ordinary differential equations describing the evolution of the locations of the pulses, or, alternatively, the evolution of the separation distances. By analyzing the fixed points of this system, we obtain bound states of interacting pulses. For two pulses, we provide a criterion for the existence of a countable infinite or finite number of bound states, depending on the strength of the dispersive term in the equation. The interaction theory and resulting bound states are corroborated by computations of the full equation. We also find qualitative agreement between the theory and the experiments.

© 2010 Elsevier B.V. All rights reserved.

1. Introduction

A thin liquid film flowing down a vertical fibre is always unstable and spontaneously breaks up into a droplike wavetrain. The studies by Frenkel [1] and Kalliadasis and Chang [2] have shown that this instability is mainly triggered by the capillary pressure induced by the azimuthal curvature (“Rayleigh–Plateau instability”); on the other hand, the pressure induced by the axial curvature is stabilizing. Streamwise viscous diffusion plays a dispersive role and affects significantly the wave selection, speeds and shapes

[3,4], while for sufficiently large flow rates inertia is present and its role is destabilizing.

This system is an example of a nonlinear active–dispersive–dissipative medium with instability/energy supply, stability/energy dissipation and dispersion. Due to its simplicity it offers an excellent opportunity for the experimental study of several generic features of the nonlinear dynamics of open-flow hydrodynamic and other nonlinear systems. For example, as was demonstrated by Duprat et al. [3], the instability can be either absolute or convective, depending on the undisturbed film thickness/flow rate. In the absolute case (for intermediate ranges of film thicknesses), a regular wave regime is observed all along the fibre: the interface typically develops a nonlinear wavetrain in which waves propagate with the same amplitude and speed (a “nonlinear global mode”). In the convective case (for large/small film thicknesses), the wave evolution is irregular and the above regular regime is never observed.

* Corresponding author. Tel.: +44 0 20 759 41373.

E-mail addresses: d.tseluiko@imperial.ac.uk (D. Tseluiko), s.saprykin@imperial.ac.uk (S. Saprykin), duprat@fast.u-psud.fr (C. Duprat), fred@fast.u-psud.fr (F. Giorgiutti-Dauphiné), s.kalliadasis@imperial.ac.uk (S. Kalliadasis).

The interface is now dominated by droplike solitary pulses which continuously interact with each other and numerous inelastic coalescence events between the pulses take place. In such events, larger pulses catch up with smaller ones and annihilate them. However, under certain conditions and when the Rayleigh–Plateau instability competes with the viscous dispersive effects (the map of the different flow regimes in the parameter space has been delineated in [5]) no more coalescence events occur after a certain distance down the fibre, and the interface is characterized by quasi-equilibrium solitary pulses which interact with each other through attractions/repulsions. For sufficiently large dispersion these quasi-equilibrium pulses form bound states. In this article, we provide a qualitative theoretical explanation of these experimentally observed phenomena by using a simple model for the flow, the so-called “generalized Kuramoto–Sivashinsky” (gKS) equation, obtained asymptotically with a long-wave expansion of the full governing equations and associated boundary conditions.

The gKS equation is one of the simplest prototypes modeling a nonlinear active medium with energy supply, energy dissipation and dispersion and whose dynamics is dominated by localized nonlinear pulses. In addition to flows down vertical fibres, this equation has been derived asymptotically from the full governing equations and associated boundary conditions in many other physical contexts, including plasma waves with dispersion due to finite ion banana width [6] and liquid films in different settings, i.e. from a film falling down a planar substrate or an inclined substrate [7–10] to films in the presence of various additional effects and complexities, e.g. films sheared by a turbulent gas [11], falling liquid films in the presence of a viscous stress at the free surface [12], liquid films flowing down a uniformly heated wall [13] and reactive falling films [14]. We note, that unlike all these studies where specific orders-of-magnitude assignments for the length/time scales were assumed a priori, the study by Frenkel and Indireskumar [7] did not assume any specific scalings a priori. Finally, we note that to rigorously justify formal asymptotic reductions to weakly nonlinear models, one needs to show that the solution of the weakly nonlinear models approaches that of the full equations in the region of validity of the models. In this direction, a noteworthy study is that of Uecker [15] who provided a partial justification of the usual (dispersionless) Kuramoto–Sivashinsky (KS) equation for film flow down an inclined plane by proving that the solutions of the KS equation approximate the solutions of the so-called “integral-boundary-layer” model (e.g. [9,10]) for the flow over sufficiently long time scales.

The paper is organized as follows. In Section 2 we describe the experiments on viscous liquid films coating vertical fibres. In Section 3 we give a detailed derivation of the gKS equation for flows down vertical fibres starting from the full Navier–Stokes equations and the corresponding wall and free-surface boundary conditions. In Section 4 we discuss a weak-interaction theory for the gKS equation and analyze bound-state formation of solitary pulses for this equation. In Section 5 we compare the theoretical results with computations. Section 6 is devoted to discussion of theoretical results, their relevance to experiments and conclusions.

2. Experimental motivation: a thin film coating a vertical fibre

A sketch of the experimental set-up is shown in Fig. 1(a). A Rhodorsil silicon oil v50 of density $\rho = 963 \text{ kg/m}^3$, dynamic viscosity $\mu = 48 \times 10^{-3} \text{ Pa s}$ and surface tension $\gamma = 20.8 \times 10^{-3} \text{ N/m}$ at 25°C flows down vertical Nylon fibres of 1.5 m length and of various radii R . To ensure strong curvature effects, required for the formation of axisymmetric droplike pulses, fibre radii are chosen to be sufficiently small, i.e. $0.2 \text{ mm} < R < 0.475 \text{ mm}$. For sufficiently large radii, axisymmetry can break down resulting in a more complicated free surface as now non-axisymmetric

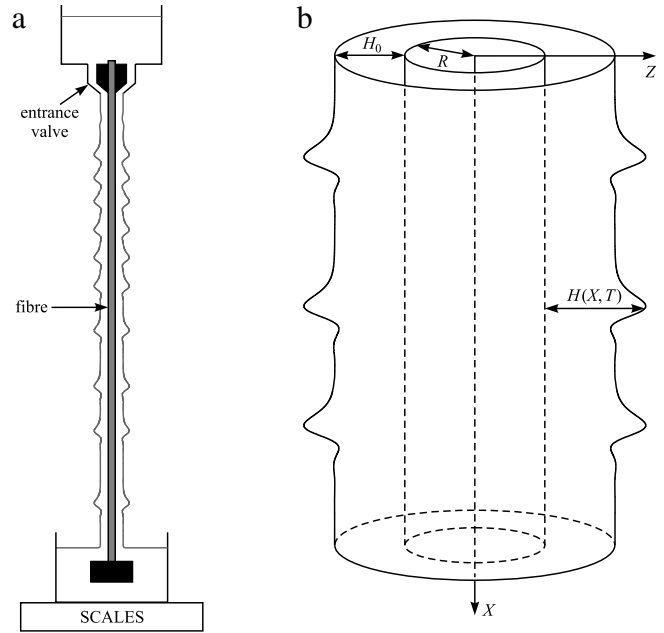


Fig. 1. (a) Experimental set-up for flow down a vertical fibre; (b) notations.

disturbances could be more unstable compared to axisymmetric ones [16]. At the same time, small radii ensure that dispersion is not very strong, i.e. the waves are characterized by small-amplitude oscillations which are crucial for the formation of bound states (for large radii only repulsions were observed experimentally). The inlet thickness H_0 (“Nusselt film thickness”) of the liquid film is controlled by the entrance valve that ensures a uniform and axisymmetric coating. We introduce a Cartesian coordinate system (X, Z) with the X -axis pointing down along the center of the fibre with $X = 0$ corresponding to the end of the entrance valve and Z being the outward-pointing coordinate normal to the fibre. The local film thickness is denoted by $H(X, T)$, where T denotes time. The flow characteristic speed is given by a balance between viscous drag and gravity, $U_0 = \rho g H_0^2 / 2\mu$, with g denoting the gravitational acceleration. The Reynolds number and the Weber number measuring the relative importance of inertia to viscosity and inertia to surface tension, respectively, are defined by:

$$\text{Re} = \frac{\rho U_0 H_0}{\mu}, \quad \text{We} = \frac{\gamma}{\rho U_0^2 H_0}. \quad (1)$$

The inlet film thickness is chosen to be $0.6 \text{ mm} < H_0 < 0.95 \text{ mm}$, which gives a U_0 of a few cm/s, $30 > \text{We} > 3$ and $0.4 < \text{Re} < 1.7$, i.e. both surface tension and viscosity effects are important. A typical profile of the resulting solitary waves is shown in Fig. 2 for $R = 0.35 \text{ mm}$, $\text{Re} = 0.59$ and $\text{We} = 16.6$. It is characterized by a sharp front preceded by a few damped oscillations and a smooth tail at the back. Surface tension and inertia lead to the development of these capillary ripples whilst viscous friction tends to suppress them. The steepening of the front is related to nonlinearities, while inertia, gravity and viscous drag are responsible for the back tail. This characteristic shape is then the signature of the main relevant features in the system, namely surface tension dissipation, viscous dispersion, inertia instability and nonlinearities.

Spatio-temporal diagrams are obtained with a linear camera following a vertical pixel line with time. A typical example of the natural (noise-driven) dynamics is depicted in Fig. 3(a) for $R = 0.35 \text{ mm}$ and $H_0 = 0.85 \text{ mm}$, giving $\text{We} = 5$ and $\text{Re} = 1.2$. The behavior is qualitatively similar for larger We and smaller R . A primary quasi-regular wavetrain is destabilized by numerous coalescence and capillary drainage enhanced repulsions, leading to

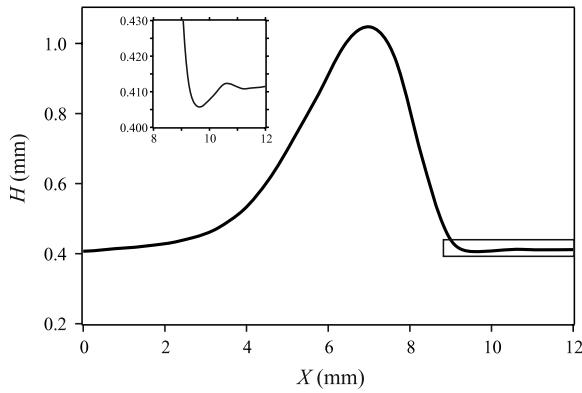


Fig. 2. Typical experimental profile of a solitary pulse.

the formation of quasi-equilibrium pulses, as shown in Fig. 3(a). After a certain distance from the inlet, typically 80 cm, no more coalescence occurs and the quasi-equilibrium pulses only rearrange themselves through interactions without exchanging mass. Such interactions are illustrated in Fig. 3(a), where **A** shows repulsion and **B** shows attraction. Neighboring pulses attract or repel each other until they are at a specific distance at which they form bound states. These bound states are also captured by imposing a weak forcing at the inlet so that the flow synchronizes faster to its long-time asymptotic state. A vibrating device is used to produce periodic pressure perturbations just above the entrance valve in the tank. The frequency and the amplitude of the perturbations are adjusted in order to produce a signal containing many harmonics. This leads to waves that rearrange through attractions and repulsions into packets of mostly two or three pulses. The rearrangement into packets of two pulses is shown in Fig. 3(b). By changing the forcing frequency and the amplitude, the pulses lock on at different distances. Detailed visualizations of attractions and repulsions are obtained with a fast digital camera; see Fig. 4 where repulsions (**A** and **C**) and attraction (**B**) are shown for flow of a 0.9 mm thick film down a fibre of radius 0.35 mm.

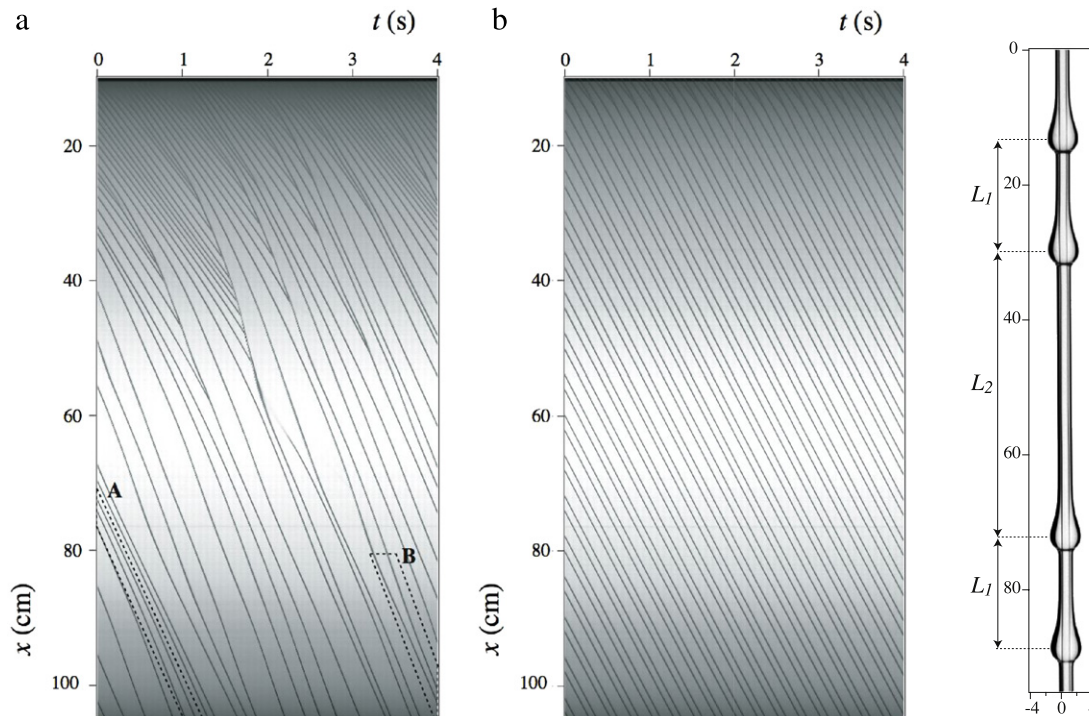


Fig. 3. (a) Natural evolution and (b) forced evolution and formation of two-pulse bound states for $R = 0.35$ mm and $H_0 = 0.85$ mm, giving $We = 5$, $Re = 1.2$ and $\delta = 0.4$. **A** and **B** in panel (a) show attractions and repulsions of the pulses, respectively.

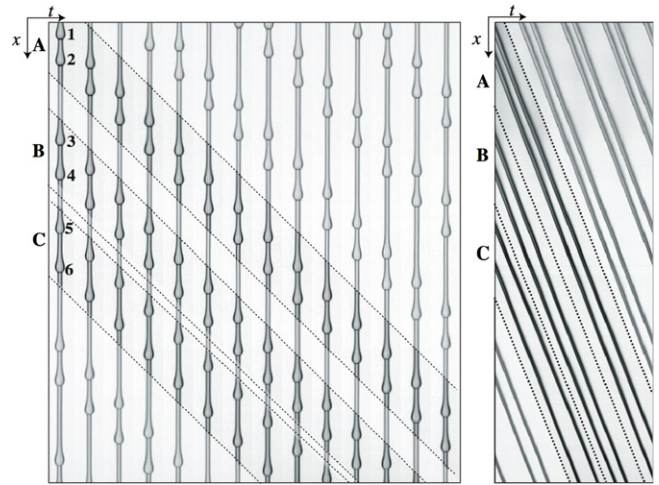


Fig. 4. Consecutive images (height: 10 cm) and the corresponding spatio-temporal diagram for natural evolution showing interactions on a fibre of radius $R = 0.35$ mm for $H_0 = 0.9$ mm ($We = 3.8$, $Re = 1.4$ and $\delta = 0.4$). **A** and **C**: repulsions and **B**: attraction. Time between two consecutive images is 0.025 s.

One might expect that for the natural dynamics the waves would rearrange in a regular fashion below a sufficient distance down the fibre. Although no obvious regular pattern is observed, statistics on the separation distances between the pulses performed at the bottom of the fibre at around $X = 1.4$ m revealed a clear reorganization of the pulses. Indeed, in the histogram presented in Fig. 5, we can observe that, although the distribution of the distances appears broad, there are four distances selected by the system which clearly stand out. We note that the interaction process is slower than the advection of the waves by the flow and a more regular rearrangement cannot be observed for the given fibre length. For the forced case, when the pulses rearrange into groups of two or three, the corresponding histograms have two peaks. Interestingly, these peaks occur at approximately the same distances

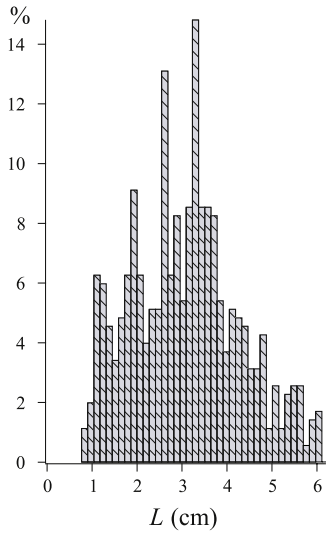


Fig. 5. Histograms of the distances at the bottom of the fibre at around $X = 1.4$ m in the natural case when $R = 0.45$ mm, $H_0 = 0.66$ mm, $We = 18$, $Re = 0.56$ and $\delta = 0.4$.

at which two of the four peaks in the histogram for the natural dynamics occur (for the same flow parameters). By changing the forcing amplitude, hence the modulation of the inlet signal, we can lock on two different distances.

3. A simple model for the flow: the gKS equation

To gain theoretical insight into the interaction of the pulses and associated formation of bound states, we assume that the free-surface profile is axisymmetric and derive a simple model for the flow through a long-wave expansion of the governing equations and wall and free-surface boundary conditions.

The governing equations are the Navier–Stokes equations written in cylindrical coordinates:

$$\rho(U_T + UU_X + VU_Z) = -P_X + \mu(U_{XX} + U_{ZZ} + U_Z/Z) + \rho g, \quad (2)$$

$$\rho(V_T + UV_X + VV_Z) = -P_Z + \mu(V_{XX} + V_{ZZ} + V_Z/Z - V/Z^2), \quad (3)$$

$$U_X + V_Z + V/Z = 0, \quad (4)$$

where U and V denote the X - and the Z -component of the velocity, respectively, and P denotes the deviation of the pressure from the atmospheric level.

At the fibre, $Z = R$, no-slip and no-penetration conditions are satisfied:

$$U = V = 0. \quad (5)$$

At the free surface, $Z = R + H(X, T)$, we have the kinematic compatibility and the tangential and normal stress balance conditions:

$$H_T + UH_X - V = 0, \quad (6)$$

$$(1 - H_X^2)(U_Z + V_X) + 2H_X(V_Z - U_X) = 0, \quad (7)$$

$$P = \frac{2\mu}{1 + H_X^2} [-H_X(U_Z + V_X) + U_X H_X^2 + V_Z] - \frac{\gamma}{(1 + H_X^2)^{3/2}} \left[H_{XX} - \frac{1 + H_X^2}{R + H} \right]. \quad (8)$$

To non-dimensionalize the equations, we choose H_0 as the length scale, $U_0 \equiv \rho g h_0^2 / 2\mu$ as the velocity scale, H_0 / U_0 as the time scale, and ρU_0^2 as the pressure scale. The equations and the boundary conditions take the following form (note that for simplicity we use the same symbols for the dimensionless variables as for the dimensional ones assuming that from now on all the variables are dimensionless):

$$U_T + UU_X + VU_Z = -P_X + \frac{1}{Re}(U_{XX} + U_{ZZ} + U_Z/Z) + \frac{2}{Re}, \quad (9)$$

$$V_T + UV_X + VV_Z = -P_Z + \frac{1}{Re}(V_{XX} + V_{ZZ} + V_Z/Z - V/Z^2), \quad (10)$$

$$U_X + V_Z + V/Z = 0. \quad (11)$$

Also, $U = V = 0$ at $Z = R^* \equiv R/H_0$, and

$$H_T + UH_X - V = 0, \quad (12)$$

$$(1 - H_X^2)(U_Z + V_X) + 2H_X(V_Z - U_X) = 0, \quad (13)$$

$$P = \frac{2}{Re(1 + H_X^2)} [-H_X(U_Z + V_X) + U_X H_X^2 + V_Z] - \frac{We}{(1 + H_X^2)^{3/2}} \left[H_{XX} - \frac{1 + H_X^2}{R^* + H} \right], \quad (14)$$

at $Z = R^* + H(X, T)$, where Re and We are the Reynolds and the Weber number, respectively, defined above by (1).

The non-dimensionalized base solution for $H(X, T) \equiv 1$ is the following:

$$\bar{U} = (R^* + 1)^2 \log \frac{Z}{R^*} - \frac{1}{2}(Z^2 - R^{*2}), \quad \bar{V} \equiv 0, \quad (15)$$

$$\bar{P} \equiv \frac{We}{R^* + 1}. \quad (16)$$

Next, we expand around the base solution, i.e. we write $U = \bar{U} + \tilde{U}$ and $P = \bar{P} + \tilde{P}$. Also, we assume long waves, i.e. we write $X = \xi/\epsilon$, $T = \tau/\epsilon$ and $V = \epsilon W$, where $\epsilon \ll 1$ is the so-called long-wave or thin-film parameter, usually defined as the ratio of the typical film thickness to the length scale over which variations in the streamwise direction occur; see e.g. [9,10]. For simplicity, we also introduce a new radial coordinate, $\zeta = Z - R^*$ and we write $R^* = \bar{R}/\epsilon$ and $We = \bar{We}/\epsilon^2$. We obtain,

$$\begin{aligned} \epsilon \tilde{U}_\tau + \epsilon(\bar{U} + \tilde{U})\tilde{U}_\xi + \epsilon W(\bar{U}' + \tilde{U}_\zeta) \\ = -\epsilon \tilde{P}_\xi + \frac{1}{Re} \left(\epsilon^2 \tilde{U}_{\xi\xi} + \tilde{U}_{\zeta\zeta} + \frac{\tilde{U}_\zeta}{\bar{R}/\epsilon + \zeta} \right), \end{aligned} \quad (17)$$

$$\begin{aligned} \epsilon^2 W_\tau + \epsilon^2(\bar{U} + \tilde{U})W_\xi + \epsilon^2 WW_\zeta \\ = -\tilde{P}_\zeta + \frac{1}{Re} \left(\epsilon^3 W_{\xi\xi} + \epsilon W_{\zeta\zeta} + \frac{\epsilon W_\zeta}{\bar{R} + \zeta} - \frac{\epsilon W}{(\bar{R}/\epsilon + \zeta)^2} \right), \end{aligned} \quad (18)$$

$$\tilde{U}_\xi + W_\zeta + \frac{W}{\bar{R}/\epsilon + \zeta} = 0. \quad (19)$$

Also, $\tilde{U} = W = 0$ at $\zeta = 0$, and

$$H_\tau + (\bar{U} + \tilde{U})H_\xi - W = 0, \quad (20)$$

$$(1 - \epsilon^2 H_\xi^2)(\bar{U}' + \tilde{U}_\zeta + \epsilon^2 W_\xi) + 2\epsilon^2 H_\xi(W_\zeta - \tilde{U}_\xi) = 0, \quad (21)$$

$$\begin{aligned} \tilde{P} = \frac{2}{Re(1 + \epsilon^2 H_\xi^2)} [-\epsilon H_\xi(\bar{U}' + \tilde{U}_\zeta + \epsilon^2 W_\xi) \\ + \epsilon^3 U_\xi H_\xi^2 + \epsilon W_\zeta] - \frac{\bar{We}}{\epsilon^2(1 + \epsilon^2 H_\xi^2)^{3/2}} \\ \times \left[\epsilon^2 H_{\xi\xi} + \frac{(1 + \epsilon^2 H_\xi^2)^{3/2}}{\bar{R}/\epsilon + 1} - \frac{1 + \epsilon^2 H_\xi^2}{\bar{R}/\epsilon + H} \right], \end{aligned} \quad (22)$$

at $\zeta = H(\xi, \tau)$.

Our first aim is to derive an evolution equation for the free surface. To do this, we expand

$$\tilde{U} = u_0 + \epsilon u_1 + \epsilon^2 u_2 + \dots, \quad (23)$$

$$W = w_0 + \epsilon w_1 + \epsilon^2 w_2 + \dots, \quad (24)$$

$$\tilde{P} = p_0 + \epsilon p_1 + \epsilon^2 p_2 + \dots. \quad (25)$$

We assume that Re , $\overline{\text{We}}$ and \overline{R} are all $O(1)$. At leading order, we obtain the system

$$u_{0\zeta\zeta} = 0, \quad p_{0\zeta} = 0, \quad w_{0\zeta} = 0, \quad (26)$$

with $u_0 = w_0 = 0$ at $\zeta = 0$ and

$$u_{0\zeta} = -\overline{U}', \quad p_0 = -\overline{\text{We}} \left[H_{\xi\xi} + \frac{H-1}{\overline{R}^2} \right] \quad (27)$$

at $\zeta = H$. The solution is:

$$\begin{aligned} u_0 &= 2(H-1)\zeta, & w_0 &= -H\zeta^2, \\ p_0 &= -\overline{\text{We}} \left[H_{\xi\xi} + \frac{H-1}{\overline{R}^2} \right]. \end{aligned} \quad (28)$$

In a similar way, we find u_1 , w_1 and p_1 by solving the system at first order and then u_2 , w_2 and p_2 by solving the system at second order. This has been done in Maple and for brevity we do not include the resulting expressions which turn out to be rather lengthy.

Now we can obtain an evolution equation for H up to and including terms $O(\epsilon^2)$ from the kinematic compatibility condition at the free surface written as

$$H_\tau + \frac{1}{\overline{R}/\epsilon + h} Q_\xi = 0, \quad (29)$$

where

$$\begin{aligned} Q &= \int_0^H (\overline{R}/\epsilon + \zeta) (\overline{U} + \tilde{U}) d\zeta \\ &= \int_0^H (\overline{R}/\epsilon + \zeta) (\overline{U} + u_0 + \epsilon u_1 + \epsilon^2 u_2) d\zeta + \dots \end{aligned} \quad (30)$$

Thus, we obtain the following equation up to $O(\epsilon^2)$:

$$H_\tau + \frac{1}{\overline{R}/\epsilon + h} \left(\int_0^H (\overline{R}/\epsilon + \zeta) (\overline{U} + u_0 + \epsilon u_1 + \epsilon^2 u_2) d\zeta \right)_\xi = 0. \quad (31)$$

The latter integral can be easily found in Maple, and for brevity we do not show the resulting expression which also turns out to be rather lengthy. It can be verified that the higher-order terms are at most $O(\epsilon^3)$ multiplied by ξ -derivatives of H .

A simpler model can now be obtained through a weakly nonlinear expansion. Our analysis revealed that a self-consistent derivation of a weakly nonlinear model that retains surface tension dissipation, viscous dispersion and inertia instability terms is only possible when $\text{Re} = O(\epsilon)$. We then write $\text{Re} = \epsilon \overline{\text{Re}}$, where $\overline{\text{Re}} = O(1)$. A balance of terms in the weakly nonlinear limit is possible if the amplitudes are $O(\epsilon^2)$. Therefore, we write $H = 1 + \epsilon^2 \eta$ where $\eta = O(1)$. Substituting this expression into the long-wave equation (31) yields

$$\begin{aligned} \epsilon^2 \eta_\tau + \left(2\epsilon^2 + \frac{2}{3\overline{R}} \epsilon^3 - \frac{1}{6\overline{R}^2} \epsilon^4 \right) \eta_\xi + 4\epsilon^4 \eta \eta_\xi \\ + \epsilon^4 \left(\frac{8\overline{\text{Re}}}{15} + \frac{\overline{\text{We}} \overline{\text{Re}}}{3\overline{R}^2} \right) \eta_{\xi\xi} + 2\epsilon^4 \eta_{\xi\xi\xi} + \epsilon^4 \frac{\overline{\text{We}} \overline{\text{Re}}}{3} \eta_{\xi\xi\xi\xi} = 0, \end{aligned} \quad (32)$$

where terms of $O(\epsilon^5)$ have been neglected. As noted earlier, the terms that we neglected in the long-wave equation are at most $O(\epsilon^3)$ multiplied by ξ -derivatives of H . Therefore, these terms become $O(\epsilon^5)$ in the weakly nonlinear limit and cannot enter the nonlinear equation given above. Dividing the above equation by ϵ^2 and writing it in the moving frame

$$\xi = \chi + \left(2 + \frac{2}{3\overline{R}} \epsilon - \frac{1}{6\overline{R}^2} \epsilon^2 \right) \tau, \quad (33)$$

we find:

$$\begin{aligned} \eta_\tau + 4\epsilon^2 \eta \eta_\chi + \epsilon^2 \left(\frac{8\overline{\text{Re}}}{15} + \frac{\overline{\text{We}} \overline{\text{Re}}}{3\overline{R}^2} \right) \eta_{\chi\chi} \\ + 2\epsilon^2 \eta_{\chi\chi\chi} + \epsilon^2 \frac{\overline{\text{We}} \overline{\text{Re}}}{3} \eta_{\chi\chi\chi\chi} = 0. \end{aligned} \quad (34)$$

To simplify this equation, we introduce new variables

$$x = \chi/A, \quad t = \tau/B, \quad h = \eta/C, \quad (35)$$

where

$$\begin{aligned} A &= \left(\frac{8}{5\overline{\text{We}}} + \frac{1}{\overline{R}^2} \right)^{-1/2}, & B &= \frac{4A^4}{\epsilon^2 \overline{\text{We}} \overline{\text{Re}}}, \\ C &= \frac{\overline{\text{We}} \overline{\text{Re}}}{12A^3}, \end{aligned} \quad (36)$$

and we obtain the following equation:

$$h_t + hh_x + h_{xx} + \delta h_{xxx} + h_{xxxx} = 0, \quad (37)$$

where

$$\delta = \frac{6A}{\overline{\text{We}} \overline{\text{Re}}} = \frac{6}{\overline{\text{We}} \overline{\text{Re}}} \left(\frac{8}{5\overline{\text{We}}} + \frac{H_0^2}{R^2} \right)^{-1/2}. \quad (38)$$

Eq. (37) is the gKS equation. It is the simplest possible nonlinear evolution prototype that retains the fundamental elements of any nonlinear active–dispersive–dissipative medium: the dominant nonlinear term hh_x , instability and energy production h_{xx} , stability and energy dissipation h_{xxxx} and dispersion δh_{xxx} . As far as the nonlinearity is concerned, its functional form can be easily obtained from symmetry considerations: indeed, the only other dominant quadratic nonlinearity is h^2 , which is obviously ruled out for systems whose spatial average does not drift, i.e. $d\langle h \rangle_x / dt = 0$.

In the limit $\delta \rightarrow 0$, the equation reduces to the usual KS equation, first derived by Homsy [17], Lin [18] and Nepomnyashchy [19] independently with a weakly nonlinear expansion for small-amplitude falling-film waves in the limiting case of large surface tension and away from criticality (when the Reynolds number is sufficiently larger than its critical value). The same equation was also obtained later in a wide variety of applications such as chemical physics/reaction–diffusion systems, e.g. propagation of concentration waves [20,21] and combustion, e.g. flame-front instabilities [22]. On the other hand, in the limit $\delta \rightarrow \infty$, the gKS equation reduces to the Korteweg–de Vries (KdV) one. This can be easily seen by introducing the change of variables in Eq. (37)

$$\tau = \delta t, \quad \tilde{h} = \frac{1}{\delta} h, \quad (39)$$

to write it as

$$\tilde{h}_t + \tilde{h} \tilde{h}_x + \tilde{h}_{xxx} + \varepsilon (\tilde{h}_{xx} + \tilde{h}_{xxxx}) = 0, \quad (40)$$

where $\varepsilon = 1/\delta$. In the limit $\varepsilon \rightarrow 0$ (or, equivalently, $\delta \rightarrow \infty$), Eq. (40) reduces to the KdV equation. The properties of the solution of Eq. (40) for small but finite ε have been scrutinized by Christov and Velarde [23].

It is well known that for small δ the gKS equation exhibits complicated chaotic dynamics in both space and time. However, a sufficiently large δ arrests the spatio-temporal chaos such that the solution evolves into a regular array of pulses that interact indefinitely with each other through their tails. This was first shown by Kawahara [24] and is illustrated in Fig. 6. More specifically, in Fig. 6(a), the temporal evolution of h is shown for $\delta = 0$. It is evident that there is no regularity and no formation of organized behavior, i.e. we get the usual KS chaos. Fig. 6(b) depicts the temporal evolution of h for $\delta = 2$. The large-time dynamics is now characterized by a row of quasi-equilibrium pulses of roughly the same shape and speed, and, therefore, it is feasible to consider the solution as a superposition of such pulses and to develop a weak-interaction theory of such pulses, as will be discussed next.

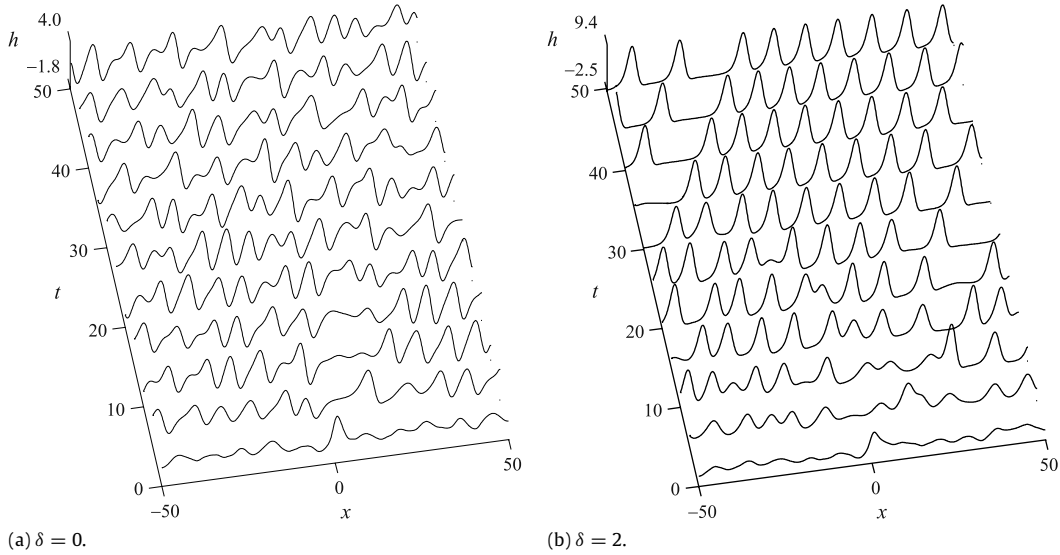


Fig. 6. Spatio-temporal evolution for h and two different values of δ . (a) $\delta = 0$: KS chaos. (b) $\delta = 2$: evolution towards a regular row of pulses. By increasing δ further and since the gKS equation starts approaching the KdV one, each pulse in the row of pulses characterizing the large-time dynamics starts approaching a KdV soliton.

4. Weak interaction and bound-state formation of the gKS pulses

In a frame moving with the velocity c_δ of a pulse, Eq. (37) becomes

$$h_t - c_\delta h_x + hh_x + h_{xx} + \delta h_{xxx} + h_{xxxx} = 0. \quad (41)$$

Let $h_0 = h_0(x)$ be a stationary pulse, satisfying the steady version of Eq. (41) and tending to zero at infinity. A detailed review of computational methodologies for localized nonlinear structures is given by Champneys and Sandstede [25].

It can be shown that $h_0(x)$ tends to zero exponentially and monotonically as $x \rightarrow -\infty$ and it tends to zero exponentially either in an oscillatory manner or monotonically as $x \rightarrow \infty$, depending on whether δ is below or above a threshold value $\delta^* \approx 3.71$ (see [26]). More specifically, $h_0(x) \sim C_1 e^{\lambda_1 x}$ as $x \rightarrow -\infty$ and $h_0(x) \sim \text{Re}(C_2 e^{\lambda_2 x})$ as $x \rightarrow \infty$, where C_1 is a real constant and C_2 is, in general, a complex one. Here, λ_1 and λ_2 are non-zero roots of the following characteristic equation:

$$\lambda^3 + \delta \lambda^2 + \lambda - c_\delta = 0. \quad (42)$$

As was shown by Kawahara and Toh [26], for any value of δ there is one root that is real and positive, which we denote by λ_1 . If δ is below the threshold value δ^* , there is a pair of complex conjugate roots, λ_2 and $\bar{\lambda}_2$, with negative real parts. Otherwise, if δ is above δ^* , there are two real roots with negative real parts. In this case, we denote the root with larger real part by λ_2 .

As noted in the previous section, computational experiments show that for sufficiently large δ the dynamics is dominated by pulses that slowly repel and attract each other. Therefore, we assume that at a particular time the solution, h , is described as a superposition of n quasi-stationary pulses h_1, \dots, h_n located at $x_1(t), \dots, x_n(t)$, respectively, namely,

$$h_i(x, t) = h_0(x - x_i(t)), \quad i = 1, \dots, n, \quad (43)$$

and a small overlap (or correction) function, $\hat{h} = \hat{h}(x, t)$, i.e. we take on the following ansatz:

$$h = \sum_{i=1}^n h_i + \hat{h}, \quad (44)$$

and derive a system of equations governing the locations of the pulses by following weak-interaction approaches implemented for other systems by Ei [27] and Sandstede [28], for example. As far as the gKS equation is concerned, previous efforts to develop weak-interaction approaches, include [29,30,8], that, however,

overlooked certain important details, as will be briefly discussed below. We also note that rigorous justifications of weak-interaction theories can be obtained by proving the existence of center manifolds formed by pulse packets. This has been done for certain cases when the primary pulse is spectrally stable; see [27,31], for instance. In the present study, however, the primary pulse is inherently unstable, and a rigorous justification of the weak-interaction results does not follow from previous studies and is left as a topic for further investigation. Nevertheless, an extensive numerical study presented in Section 5 provides a strong evidence of the validity of the weak-interaction theory for the gKS equation. We also note that some rigorous analytical results to explain the persistence of gKS pulses and their interaction in the limit of large δ were obtained by Pego et al. [32]. Finally, we note that renormalization group techniques have been used to capture the leading-order pulse motion for well-separated pulses, for example, for the nonlinear Schrödinger equation, e.g. [33].

A detailed construction of the weak-interaction theory for the gKS pulses will be reported in a separate study. Formal application of this theory leads to the following system describing the leading-order dynamics of the locations of the pulses:

$$x'_1 = \int_{-\infty}^{\infty} (h_1 h_2)_x \Psi^1 dx, \quad (45)$$

$$x'_i = \int_{-\infty}^{\infty} (h_{i-1} h_i)_x \Psi^i dx + \int_{-\infty}^{\infty} (h_i h_{i+1})_x \Psi^i dx, \quad 1 < i < n, \quad (46)$$

$$x'_n = \int_{-\infty}^{\infty} (h_{n-1} h_n)_x \Psi^n dx, \quad (47)$$

where $\Psi^i(x, t) = \Psi^0(x - x_i(t))$ and Ψ^0 is a non-constant function belonging to the null space of the operator adjoint to the one obtained by linearizing (41) around the pulse h_0 . We normalize it so that $\int_{-\infty}^{\infty} h_{0x} \Psi^0 dx = 1$. Our analysis revealed that Ψ^0 exists and has a jump at infinity. The existence of such a function, also noticed by Elphick et al. [29], implies that the localized function in the null space of the adjoint operator given by Chang and Demekhin [8] and postulated by Ei and Ohta [30] is erroneous.

Using the notations

$$S_1(l) \equiv - \int_{-\infty}^{\infty} h_0(x + l/2) h_0(x - l/2) \Psi_x^0(x + l/2) dx, \quad (48)$$

$$S_2(l) \equiv - \int_{-\infty}^{\infty} h_0(x + l/2) h_0(x - l/2) \Psi_x^0(x - l/2) dx. \quad (49)$$

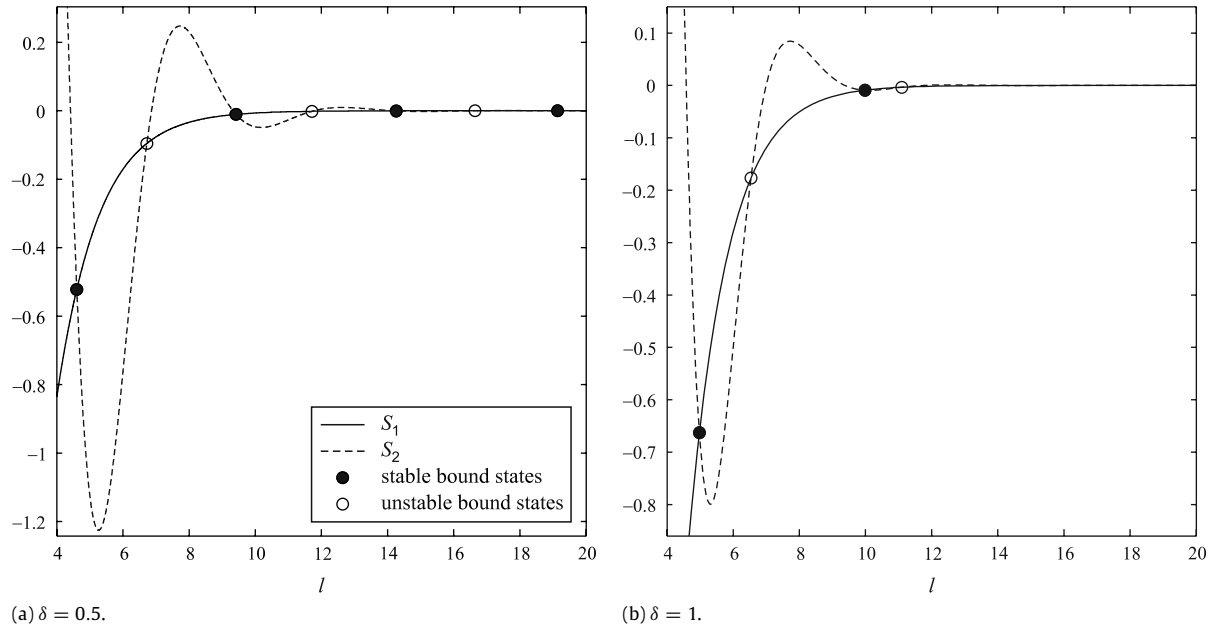


Fig. 7. Dependence of S_1 and S_2 on the separation distance between two pulses (solid and dashed lines, respectively) for $\delta = 0.5$ and 1 (panels (a) and (b), respectively). The intersection points are shown as circles. Black circles correspond to stable two-pulse bound states. Empty circles correspond to unstable two-pulse bound states.

we can write

$$x'_1 = S_1(x_2 - x_1), \quad (50)$$

$$x'_i = S_2(x_i - x_{i-1}) + S_1(x_{i+1} - x_i), \quad 1 < i < n, \quad (51)$$

$$x'_n = S_2(x_n - x_{n-1}). \quad (52)$$

This system can be extended to an infinite one for an infinite array of pulses: $x'_i = S_2(x_i - x_{i-1}) + S_1(x_{i+1} - x_i)$, for $i \in \mathbb{Z}$.

Noting that $l'_i = x'_{i+1} - x'_i$, $i = 1, \dots, n-1$, (50)–(52) can be transformed to the following coupled system of ordinary differential equations for the separation distances l_i 's:

$$l'_1 = S_2(l_1) + S_1(l_2) - S_1(l_1), \quad (53)$$

$$l'_i = S_2(l_i) + S_1(l_{i+1}) - S_2(l_{i-1}) - S_1(l_i), \quad 1 < i < n-1, \quad (54)$$

$$l'_{n-1} = S_2(l_{n-1}) - S_2(l_{n-2}) - S_1(l_{n-1}). \quad (55)$$

For a bound state of n pulses, the distances l_i , $i = 1, \dots, n-1$, for which the bound state can be formed, must be stationary, i.e. the following nonlinear system must be satisfied:

$$S_2(l_1) + S_1(l_2) - S_1(l_1) = 0, \quad (56)$$

$$S_2(l_i) + S_1(l_{i+1}) - S_2(l_{i-1}) - S_1(l_i) = 0, \quad 1 < i < n-1, \quad (57)$$

$$S_2(l_{n-1}) - S_2(l_{n-2}) - S_1(l_{n-1}) = 0. \quad (58)$$

For instance, for a bound state of two pulses we must have $S_1(l_1) = S_2(l_1)$. The graphs of S_1 and S_2 are shown in Fig. 7 for $\delta = 0.5$ and 1 (see panels (a) and (b), respectively). The abscissas of the intersection points indicate distances for which bound states can be formed, and the ordinates indicated the corresponding velocities of the bound states relative to c_δ . Black and empty circles correspond to stable and unstable bound states, respectively. Consider, for example, the first bound state at $l \approx 5$. For $l \gtrsim 5$, $S_1 > S_2$ or $x'_1 > x'_2$ so that the first pulse moves faster than the second one which then leads to l decreasing. On the other hand, for $l \lesssim 5$, $x'_1 < x'_2$, leading to l increasing. It is also interesting to note that the ordinates of the intersection points are always negative, i.e. the velocity of a two-pulse bound state is always less than that of an individual pulse. Another interesting observation is that for $\delta = 0.5$ we, apparently, get a countable infinite number of bound states, whilst for $\delta = 1$

there are only four possible bound states—two stable and two unstable. This can be justified analytically by showing that $S_1(l) \sim D_1 e^{-\lambda_1 l}$, $S_2(l) \sim \text{Re}(D_2 e^{\lambda_2 l})$ as $l \rightarrow \infty$, where D_1 is a real constant and D_2 is, in general, a complex number. Recall that λ_1 is the real positive root of (42) and λ_2 is the root of (42) with a maximum negative real part. Since λ_1 is always real, S_1 tends to zero in a monotonic manner as $l \rightarrow \infty$. Also, λ_2 has a non-zero imaginary part iff $\delta < \delta^* \approx 3.71$ meaning that S_2 tends to zero either in an oscillatory or monotonic manner depending on whether $\delta < \delta^*$ or $\delta \geq \delta^*$. Thus, if $\lambda_1 + \text{Re}\lambda_2 > 0$, there exists a countable infinite number of two-pulse bound states. Otherwise, if $\lambda_1 + \text{Re}\lambda_2 < 0$, there exists a finite number of two-pulse bound states (or no bound states at all).

It is interesting to note that the latter criterion for the existence of a countable infinite or finite number of two-pulse bound states coincides exactly with the Shilnikov criterion for the existence of an infinite countable or finite number of subsidiary homoclinic orbits (see [34] for example). However, the approach adopted in the present work not only provides an existence result for bound states, but also gives the description of the dynamics of the pulses. Further, it can be extended to higher dimensions and could in principle be applied to non-local PDEs where the Shilnikov-type approach is not applicable.

The calculations for the gKS equation show that $\lambda_1 + \text{Re}\lambda_2 < 0$ iff $\delta < \tilde{\delta} \approx 0.85$. This explains why there is a countable infinite number of two-pulse bound states for $\delta = 0.5$ and a finite number for $\delta = 1$, as is illustrated in Fig. 7. For $\delta = 0.5$, the pulse separation distance will tend to the nearest stable bound-state separation distance. The same is true for $\delta = 1$, unless the initial separation distance is above the threshold value of about 11, beyond which the pulse dynamics will be repulsive. The repulsive dynamics for large δ was noticed by Kawahara and Toh [26] and Chang and Demekhin [8]. We also note that Kawahara and Toh [26] using their approach claimed that there were no bound states for $\delta = 1$. Our result, however, clearly indicates the possible existence of two stable and two unstable bound states; see Fig. 7(b) (and the existence of a stable bound state with the separation distance of approximately 10 has been confirmed by our time-dependent computations to be discussed in the next section).

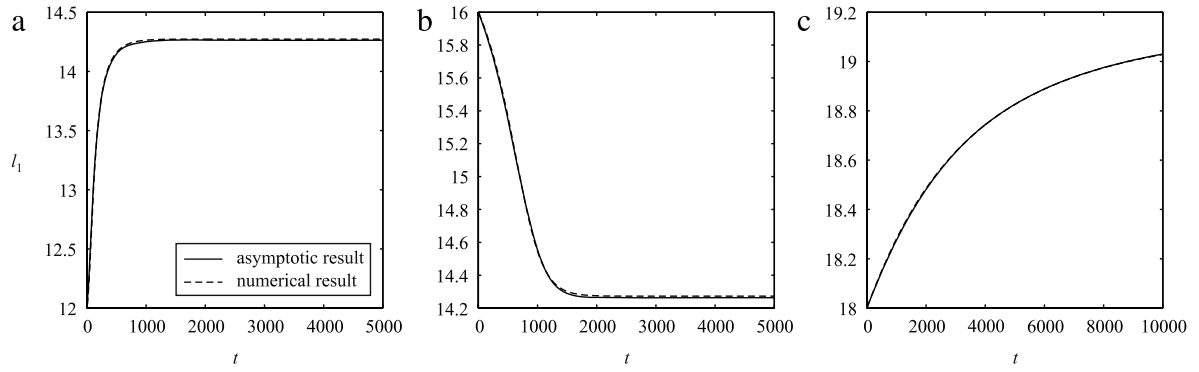


Fig. 8. Dependence of the pulse separation distance on time for $\delta = 0.5$. Panels (a), (b) and (c) show the evolution of the two-pulse separation distance when the initial separation distances are 12, 16 and 18, respectively. Solid lines are obtained by solving numerically the model in (59). Dashed lines are obtained by solving numerically the gKS equation with a superposition of two pulses as an initial condition.

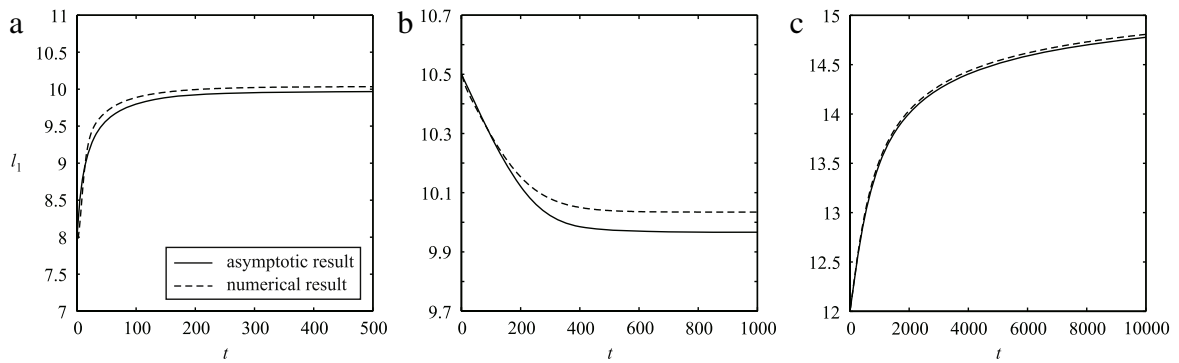


Fig. 9. Dependence of the pulse separation distance on time for $\delta = 1$. Panels (a), (b) and (c) show the evolution of the two-pulse separation distance when the initial separation distances are 8, 10.5 and 12, respectively. Solid lines are obtained by solving numerically the model in (59). Dashed lines are obtained by solving numerically the gKS equation with a superposition of two pulses as an initial condition.

5. Comparison of theory with computations

To validate the pulse-interaction theory, we compared its predictions with numerical solutions of the full time-dependent equation (41). To solve (41) numerically, we implemented a pseudospectral numerical method with a linear propagator so that the linear part of the spatial operator is done exactly in the Fourier space and the stiffness is removed (see, for example, [35]). Also, to eliminate instabilities due to numerical noise and, therefore, to track the pulse evolution for sufficiently long times, we used exponentially weighted spaces, where the primary gKS pulses are stable. The details of the numerical scheme will be reported elsewhere. For the justification of the use of exponentially weighted spaces see, for example, [36] for the KdV equation and [37] for a more general class of equations.

In Figs. 8 and 9, we present the results of computational experiments for $\delta = 0.5$ and 1, respectively, where a superposition of two pulses was taken as an initial condition. For Fig. 8(a), the initial pulse separation distance was taken to be 12. The dynamics in this case is repulsive. For Fig. 8(b), the initial pulse separation distance was taken to be 16, and the dynamics was found to be attractive. For both Fig. 8(a) and (b) the pulses tend to form a bound state with the separation distance of approximately 14.3. The solid lines in the figure were obtained by solving the model

$$l_1' = S_2(l_1) - S_1(l_1), \quad (59)$$

and we found very good agreement with the results obtained by solving (41) numerically in a weighted space with a superposition of two pulses as an initial condition (dashed lines). As the initial separation distance between the pulses is increased, the agreement becomes better, as is evident from Fig. 8(c), where the

initial separation distance was taken to be 18 (the two lines are graphically indistinguishable).

In Fig. 9 the value of δ is 1. In Fig. 9(a), the initial pulse separation distance was taken to be 8. The dynamics in this case is repulsive. In Fig. 9(b), the initial pulse separation distance was taken to be 10.5. The dynamics in this case is attractive. For both Fig. 9(a) and (b) the pulses tend to form a bound state with the separation distance of approximately 10. If the initial separation distance is larger than approximately 11, the dynamics is only repulsive. An example is given in Fig. 9(c), where the initial separation distance was taken to be 12.

Having validated the interaction theory, we performed numerical experiments for various numbers of pulses. Fig. 10 shows a typical numerical solution of (50)–(52) with the world lines tracking the locations of 24 pulses when $\delta = 0.4$. We can observe repulsions, attractions and formation of bound states of two and three pulses. Note that the world lines are shown in the frame moving with the velocity of a stationary solitary pulse. Note also the qualitative similarity with the world lines obtained in experiments on coating flows down vertical fibres shown in Fig. 3(a).

We also performed a series of numerical experiments for the gKS equation (41) in a non-weighted space, where the initial condition was a localized disturbance generated randomly. The equation was solved on a periodic domain $[-1000, 1000]$ which was discretized into 2^{14} intervals. We considered two values of δ , namely, 0.5 and 1. The initial disturbance resulted in an expanding wave packet with the envelopes traveling at a speed smaller to that of an individual solitary pulse. This in turn resulted in production of pulses escaping the expanding wave packet. For $\delta = 0.5$ and 1, it was possible to numerically propagate the solution up to approximately $t = 400$ and 285, respectively. Beyond these values

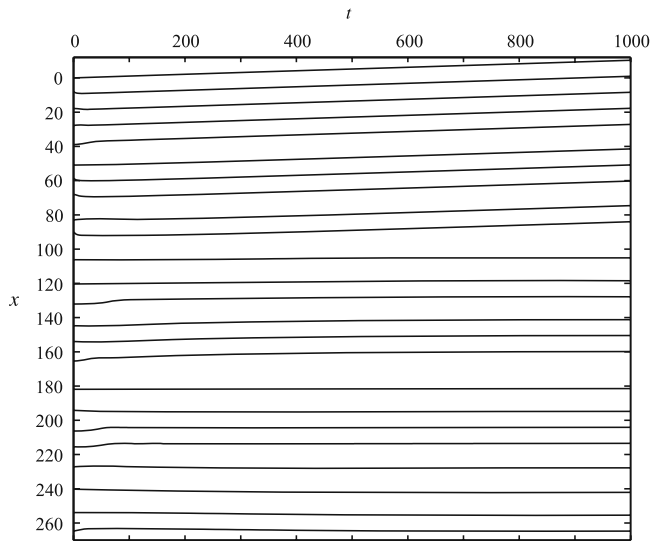


Fig. 10. Numerical solution of (50)–(52) for 24 pulses when $\delta = 0.4$. Attractions and repulsions can be observed as well as formation of bound states.

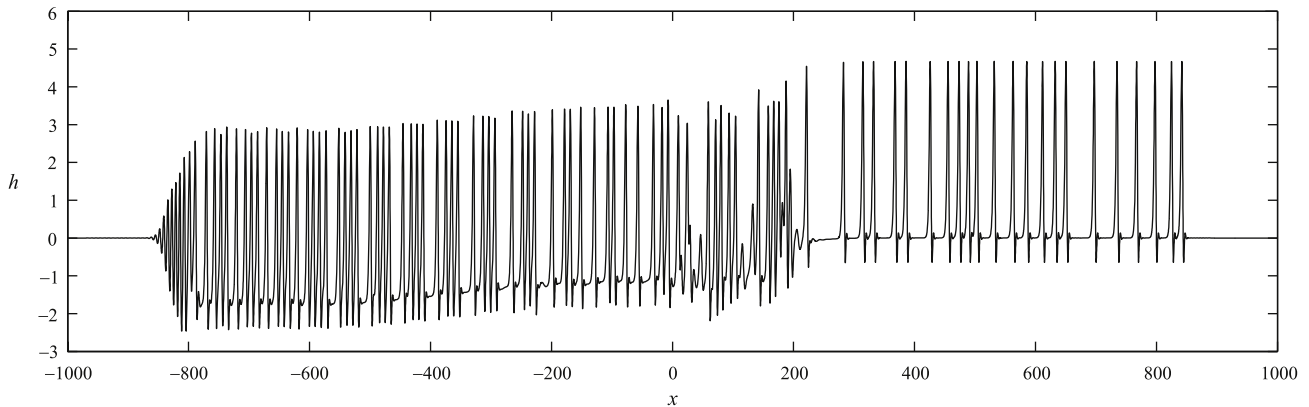
the front pulses started interacting through the period with the rear side of the expanding wave packet.

Typical outcomes are shown in Fig. 11(a) and (b) for $\delta = 0.5$ and 1, respectively. We performed 1500 numerical experiments for each δ and computed the pulse separation distance data for each case. For $\delta = 0.5$ and 1 we took into account the first 11 and 9 pulses, respectively, from each numerical experiment. In Fig. 12, we show the distributions of separation distances for

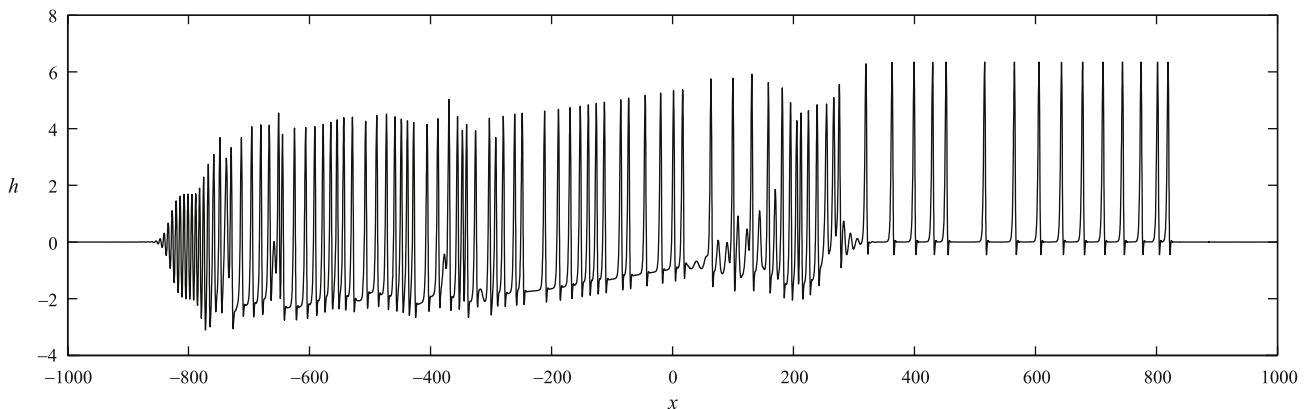
$\delta = 0.5$ at two different times, $t = 300$ and 400, panels (a) and (b), respectively, obtained by placing the distances into 60 equally spaced intervals. The distributions are multimodal for this value of δ . The first three sharp pronounced peaks occur at around $l = 9.5, 14.5$ and 18.5 , which are in good agreement with the pulse separation distances that correspond to the theoretically predicted bound states; see Fig. 7(a). Note that the occurrence of the peaks in the histogram of separation distances was also observed in experiments on coating flows down vertical fibres; see Fig. 5. We also note that as t increases, these peaks become more pronounced. In Fig. 13, we show the distribution of separation distances for $\delta = 1$ at $t = 213.75$ and 285 (panels (a) and (b), respectively). In this case, the distributions are rather unimodal and slightly skewed with thicker left tails. Although the theory predicts a possible existence of only one stable two-pulse bound state, see Fig. 7(b) (for $l \approx 10$ —the other one for $l \approx 5$ definitely does not satisfy the assumption of a “small” overlap of two pulses and does not correspond to a bound state), we do not observe a clear peak formation in the histograms in Fig. 13. However, we can still observe some thickening of the left tail of the histogram and some accumulation near $l \approx 10$, which is consistent with the theory. Also, as t increases, the peak becomes less pronounced and the left tail thickens.

6. Discussion and comparison with experiments

We have presented experimental results on the flow of a liquid film down a vertical fibre. Such flow is unstable (due to Rayleigh–Plateau instability) and the film breaks up into a droplike wavetrain. The instability can be both absolute and convective. We found that for the convective case, the primary wavetrain is



(a) $\delta = 0.5, t = 400$.



(b) $\delta = 1, t = 285$.

Fig. 11. Numerical solutions of the gKS equation on a periodic interval $[-1000, 1000]$ for $\delta = 0.5$ and 1 (panels (a) and (b), respectively) at $t = 400$ and 285, respectively.

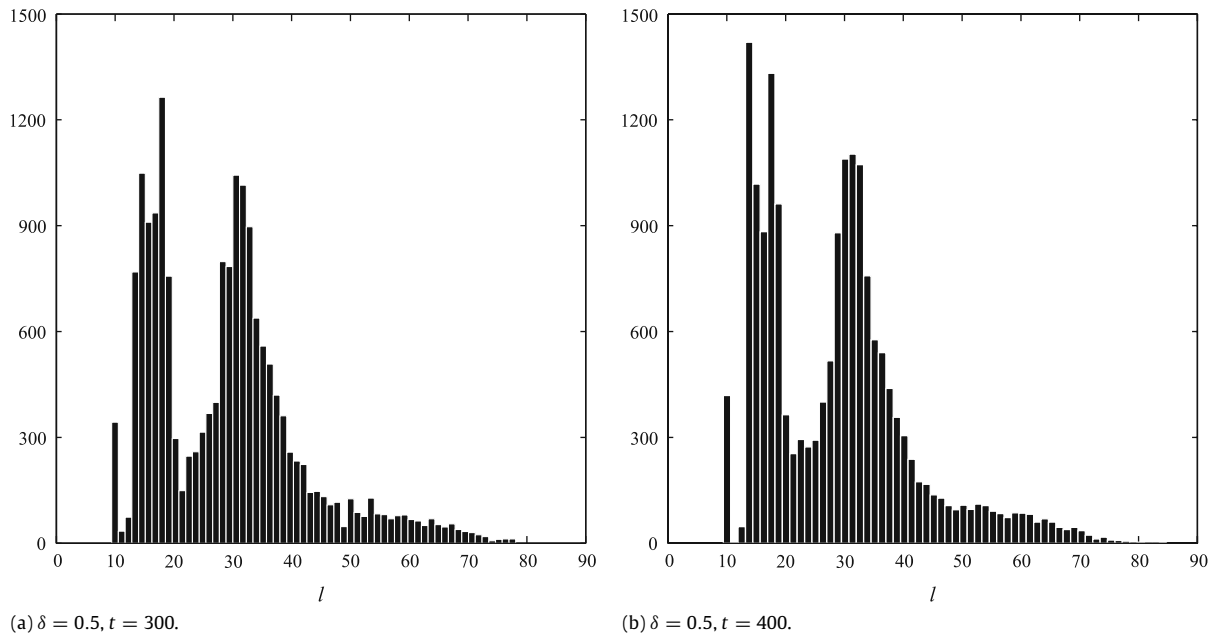


Fig. 12. Histogram for pulse separation distances based on a series of computational experiments for $\delta = 0.5$ at $t = 300$ and 400 (panels (a) and (b), respectively).

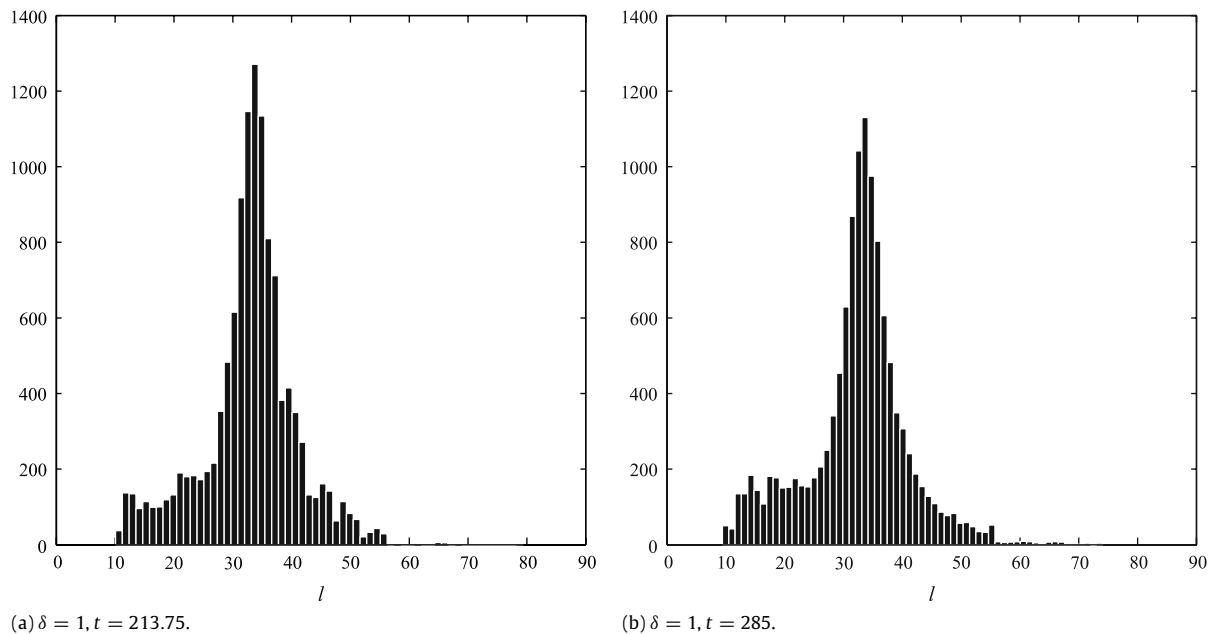


Fig. 13. Histogram for pulse separation distances based on a series of computational experiments for $\delta = 1$ at $t = 213.75$ and 285 (panels (a) and (b), respectively).

characterized by numerous coalescence events while for certain flow parameters no more coalescence events occur below a certain distance down the fibre. The film free surface is then dominated by interacting solitary pulses that either attract or repel each other. Statistical analysis of the separation distances revealed a clear reorganization of the pulses—certain distances stand out in the histogram of the pulse separation distances measured at some point at the bottom of the fibre as shown in Fig. 5.

To obtain theoretical insight into the experimentally observed phenomena, we derived a simple model for the flow, the gKS equation. The derivation is based on a long-wave expansion of the governing equations and fibre and free-surface boundary conditions. The gKS equation is one of the simplest prototypes that describes many other nonlinear active media with energy supply, dissipation, dispersion and nonlinearity. The spatio-temporal evolution of

a solution to the gKS equation is dominated by interacting localized nonlinear pulses (provided that the dispersion coefficient is sufficiently strong), just as we find in the experiments on coating flows down vertical fibres. We subsequently studied the weak interaction of solitary pulses and bound-state formation phenomena for this equation. Our theoretical approach was based on representing the solution as a superposition of such pulses and an overlap function. Under the assumption that the pulses are sufficiently separated, we obtained a dynamical system describing the evolution of the locations of the pulses.

By analyzing the fixed points of this system, we obtained bound states of pulses. In particular, we analyzed in detail bound states of two pulses. We provided a criterion for the existence of a countable infinite or finite number of bound states, depending on the strength of the dispersive term in the gKS equation. Interestingly,

this criterion exactly coincides with the Shilnikov criterion on the existence of subsidiary homoclinic orbits. However, in addition to providing an existence result for the bound states, our approach also gives the description of the dynamics of the pulses. Besides, it can be extended to higher dimensions and could in principle be applied to non-local PDEs where the Shilnikov-type approach is not applicable. Our interaction theory and resulting bound states were corroborated by computational experiments. In particular, we found that the dynamic interaction of the pulses is well described by a simplified time-dependent model obtained from the dynamical system for the location of the pulses. We can obtain both attraction and repulsion of the pulses which is in qualitative agreement with our experimental results presented in Section 2.

We have also performed a series of numerical experiments for the gKS equation on a large periodic domain with a random initial condition and collected statistics on the separation distances of the pulses. The results showed that for the values of δ for which the theory predicts bound states, the histograms of the separation distances have well-pronounced peaks occurring at values corresponding to separation distances of the stable bound states obtained by the theory. This observation is in qualitative agreement with our experiments where the histograms also manifested well-pronounced peaks (compare the histograms in Figs. 5 and 12). The value of δ which corresponds to Fig. 3 is $\delta \approx 0.4$. The theory predicts that bound states exist for this value of δ and this is consistent with our experimental observations. However, the quantitative agreement of the experimental and theoretical separation distances is not quite achieved. When we convert the theoretical bound-state separation distances into dimensional ones, we find that the experimental distances are larger than the theoretical ones by a factor of approximately 2–3. But this is to be expected since for the theory we assumed that the radius of the fibre is much larger than the film thickness, which is not the case in the experiments. Violation of this assumption affects significantly the rescaling of the distances. We further note that there are certain experimental limitations on the thickness of the film which we can use, i.e. below a critical distance no flat film can emerge close to the entrance valve. On the other hand, for larger radii we obtain large values of δ and no bound states are found both theoretically and experimentally. Thus, the best compromise to obtain bound states in the experiments and a qualitative agreement with the theory is to use a film whose thickness is of the same order as the fibre radius. Although we do not have quantitative agreement, we are still able to obtain a qualitative description of the experimentally observed phenomena as the gKS prototype contains all the important ingredients of the physical system.

Acknowledgements

We acknowledge financial support from the Engineering and Physical Sciences Research Council of the UK (EPSRC) through grant nos. EP/F009194 and EP/F016492 and the Franco-British Research Partnership Programme for a travel grant.

References

- [1] A.L. Frenkel, Nonlinear theory of strongly undulating thin films flowing down vertical cylinders, *Europhys. Lett.* 18 (1992) 583–588.
- [2] S. Kalliadasis, H.-C. Chang, Drop formation during coating of vertical fibres, *J. Fluid Mech.* 261 (1994) 136–168.
- [3] C. Duprat, C. Ruyer-Quil, S. Kalliadasis, F. Giorgiutti-Dauphiné, Absolute and convective instabilities of a viscous film flowing down a vertical fiber, *Phys. Rev. Lett.* 98 (2007) 244502.
- [4] C. Ruyer-Quil, P. Trevelyan, F. Giorgiutti-Dauphiné, C. Duprat, S. Kalliadasis, Modelling film flows down a fibre, *J. Fluid Mech.* 603 (2008) 431–462.
- [5] C. Duprat, C. Ruyer-Quil, F. Giorgiutti-Dauphiné, Spatial evolution of a film flowing down a fiber, *Phys. Fluids* 21 (2009) 042109.
- [6] B.I. Cohen, J.A. Krommes, W.M. Tang, M.N. Rosenbluth, Non-linear saturation of the dissipative trapped ion mode by mode coupling, *Nucl. Fusion* 16 (1976) 971–992.
- [7] A.L. Frenkel, K. Indreshkumar, Wavy film flows down an inclined plane: perturbation theory and general evolution equation for the film thickness, *Phys. Rev. E* 60 (1999) 4143–4157.
- [8] H.-C. Chang, E.A. Demekhin, *Complex Wave Dynamics on Thin Films*, Elsevier Scientific, 2002.
- [9] S. Kalliadasis, U. Thiele (Eds.), *Thin Films of Soft Matter*, Springer, Wien, New York, 2007.
- [10] S. Kalliadasis, C. Ruyer-Quil, B. Scheid, M.G. Velarde, *Film Flows, Wave Instabilities and Thermocapillarity*, Springer Series on Applied Mathematical Sciences (2010) (in press).
- [11] L.A. Jurman, M.J. McCready, Study of waves on thin liquid films sheared by turbulent gas flows, *Phys. Fluids A* 1 (1989) 522–536.
- [12] A. Oron, D.A. Edwards, Stability of a falling liquid film in the presence of interfacial viscous stress, *Phys. Fluids A* 5 (1993) 506–508.
- [13] S. Kalliadasis, E.A. Demekhin, C. Ruyer-Quil, M.G. Velarde, Thermocapillary instability and wave formation on a film flowing down a uniformly heated plane, *J. Fluid Mech.* 492 (2003) 303–338.
- [14] P.M.J. Trevelyan, S. Kalliadasis, Dynamics of a reactive falling film at large Péclet numbers. I. Long-wave approximation, *Phys. Fluids* 16 (2004) 3191–3208.
- [15] H. Uecker, Approximation of the integral boundary layer equation by the Kuramoto–Sivashinsky equation, *SIAM J. Appl. Math.* 63 (2003) 1359–1377.
- [16] T. Shlang, G.I. Sivashinsky, Irregular flow of a liquid film down a vertical column, *J. Phys.* 43 (1982) 459–466.
- [17] G.M. Homsy, Model equations for wavy viscous film flow, in: *Lectures in Applied Mathematics: Nonlinear Wave Motion*, vol. 15, 1974, pp. 191–194.
- [18] S.P. Lin, Finite amplitude side-band stability of a viscous film, *J. Fluid Mech.* 63 (1974) 417–429.
- [19] A.A. Nepomnyashchy, Stability of wave regimes in a film flowing down on inclined plane, *Fluid Dyn.* 9 (1974) 354–359.
- [20] Y. Kuramoto, T. Tsuzuki, On the formation of dissipative structures in reaction diffusion systems, *Prog. Theor. Phys.* 54 (1975) 687–699.
- [21] Y. Kuramoto, Diffusion-induced chaos in reaction systems, *Prog. Theor. Phys. Suppl.* 64 (1978) 346–367.
- [22] G.I. Sivashinsky, Nonlinear analysis of hydrodynamic instability in laminar flames. Part 1, *Acta Astronaut.* 4 (1977) 1176–1206.
- [23] C.I. Christov, M.G. Velarde, Dissipative solitons, *Physica D* 86 (1985) 323–347.
- [24] T. Kawahara, Formation of saturated solitons in a nonlinear dispersive system with instability and dissipation, *Phys. Rev. Lett.* 51 (1983) 381–383.
- [25] A.R. Champneys, B. Sandstede, Numerical computation of coherent structures, in: B. Krauskopf, H.M. Osinga, J. Galan-Vioque (Eds.), *Numerical Continuation Methods for Dynamical Systems*, Springer, 2007, pp. 331–358.
- [26] T. Kawahara, S. Toh, Pulse interaction in an unstable dissipative–dispersive nonlinear system, *Phys. Fluids* 11 (1988) 2103–2111.
- [27] S.-I. Ei, The motion of weakly interacting pulses in reaction–diffusion systems, *J. Dynam. Differential Equations* 14 (2002) 85–137.
- [28] B. Sandstede, Stability of travelling waves, in: B. Fiedler (Ed.), *Handbook of Dynamical Systems II*, North-Holland, 2002, pp. 983–1055.
- [29] C. Elphick, G.R. Ierley, O. Regev, E.A. Spiegel, Interacting localized structures with Galilean invariance, *Phys. Rev. A* 44 (1991) 1110–1122.
- [30] S.-I. Ei, T. Ohta, Equation of motion for interacting pulses, *Phys. Rev. E* 50 (1994) 4672–4678.
- [31] S. Zelik, A. Mielke, Multi-pulse evolution and space–time chaos in dissipative systems, *Mem. Amer. Math. Soc.* 198 (2009) 1–95.
- [32] R.L. Pego, G.S. Schneider, H. Uecker, Long-time persistence of Korteweg–de Vries solitons as transient dynamics in a model of inclined film flow, *Proc. Roy. Soc. Edinburgh Sect. A* 137 (2007) 133–146.
- [33] K. Promislow, A renormalization method for modulational stability of quasi-steady patterns in dispersive systems, *SIAM J. Math. Anal.* 33 (2002) 1455–1482.
- [34] P. Glendinning, C. Sparrow, Local and global behaviour near homoclinic orbits, *J. Stat. Phys.* 35 (1984) 645–696.
- [35] L.N. Trefethen, *Spectral Methods in Matlab*, Society for Industrial and Applied Mathematics, Philadelphia, PA, 2000.
- [36] R.L. Pego, M.I. Weinstein, Asymptotic stability of solitary waves, *Comm. Math. Phys.* 164 (1994) 305–349.
- [37] B. Sandstede, A. Scheel, Absolute and convective instabilities of waves on unbounded and large bounded domains, *Physica D* 145 (2000) 233–277.